Applied Water Science (2024) 14:25
https://doi.org/10.1007/s13201-023-02052-8

ORIGINAL ARTICLE

Photocatalytic degradation of methylene blue dye by magnetized TiO_2-silica nanoparticles from rice husk

Lekan Taofeek Popoola[1] · Adeyinka Sikiru Yusuff[1] · Aderibigbe Tajudeen Adejare[2] · Sabitu Babatunde Olasupo[3]

Received: 2 June 2023 / Accepted: 15 November 2023 / Published online: 22 January 2024

Abstract

In this current study, magnetized TiO_2-supported SiO_2 nanoparticles, synthesized from rice husk, was applied as a photocatalyst to degrade methylene blue dye (MBD) in aqueous solution using LED lamp as light source. The effects of MBD initial concentration, TiO_2 loading, pH and illumination time on the degradation efficiency of the photocatalyst on MBD was investigated using Box–Behnken design as the experimental design tool. Photocatalyst was characterized by Fourier transform infrared, scanning electron microscopy, energy-dispersive X-ray, thermogravimetric analysis and Brunauer–Emmett–Teller. At optimum predicted point where MBD initial concentration, TiO_2 loading, pH and illumination time were 10 ppm, 15%, 6 and 75 min, respectively, the predicted and experimental percentage of MBD removed were 97.66% and 96.89%, respectively. Correlation coefficient and ANOVA justified high significance of the developed model for prediction. Experimental data fitted excellently into pseudo-second-order kinetic model. The temperature effect revealed optimum MBD photocatalytic degradation at 50 °C by TiO_2/mRH-SNP. Characterization revealed the effects of magnetization and TiO_2 addition on the synthesized SiO_2 nanoparticles from rice husk. In conclusion, magnetized TiO_2-silica nanoparticles from rice husk could be effectively used to degrade MBD in solution.

Keywords Photocatalyst · Methylene blue · Box–Behnken design · Magnetized TiO_2-silica nanoparticles · Rice husk

Introduction

The increase in global population rate has greatly influenced the demand for textile products via sufficient industrialization (Thabet et al. 2022). This increases the use of synthetic dyes which simultaneously increase the volume of wastewater from dye industries such as textile manufacturing, leather making and paper printing (Tony and Mansour 2020). Our environment, both soil and water, is polluted with these synthetic dyes present in the dye wastewater. Many of the dyes are carcinogenic, toxic, soluble in water and nondegradable under atmospheric conditions (Oyewo et al. 2020; Yusuff et al. 2021). Various kinds of respiratory ailments have been linked to these dyes and their metabolites worldwide (Sumanjit and Ravneet 2007). Hence, it is imperative to design highly effective treatment plant that will handle larger volume of discharged textile wastewater and develop low cost-effective means of tackling this menace (Popoola 2019a). Of all the available techniques (Latif et al. 2010), adsorption (Lorenc-Grabowska and Gryglewicz 2007; Xiao et al. 2020) and photocatalytic degradation (Pandit et al. 2015; Li et al 2020) of organic pollutants have been identified as promising sustainable techniques of treating wastewater polluted with different kinds of dyes owing by their simplicity, low cost and highly efficient removal attributes (Lim et al. 2011).

For photocatalysis, degradation of dye component occurs via oxidation and decomposition processes on its surface with the aid of a photocatalyst, usually heterogeneous titanium dioxide (TiO_2) (Xing et al. 2016). During this process, electrons are transferred from the valence band to the conduction band of a semiconductor surface when light of an appropriate wavelength is illuminated. High oxidizing power species of hydroxide radicals and superoxide anions (which

✉ Lekan Taofeek Popoola
ltpopoola@abuad.edu.ng; popoolalekantaofeek@yahoo.com

[1] Separation Processes Research Laboratory, Chemical and Petroleum Engineering Department, Afe Babalola University, Ado-Ekiti, Ekiti State, Nigeria

[2] Science Laboratory Technology Department, Yaba College of Technology, Lagos, Lagos State, Nigeria

[3] National Agency for Food and Drug Administration and Control, Lagos, Lagos State, Nigeria

possess strong ability to degrade numerous molecules in wastewater including dye effluents) are produced as a result of reaction between the generated excitons and oxygen or water. This is called advanced oxidation process (AOP) which involves wastewater decontamination by reactive oxygen species and some other species (Gul and Yildlrln 2009; Elmorsi et al. 2010). Organic pollutants are completely mineralized to carbon dioxide, water and inorganic compounds with this process. Heterogeneous photocatalysis is one of the effective methods of AOP capable of oxidizing most of the organic carbon at ambient condition (Rashed et al. 2017). The cost effective, high stability, earth abundance oxide and non-toxicity nature of TiO_2 has greatly supported its suitability as a photocatalyst for wastewater treatment under solar-driven condition. Though large bandgap energy of TiO_2 (~3.2 eV) restricted its photoactivity to the UV region of the solar spectrum, its anatase phase strengthens its photoactivity because it possesses high photon absorption characteristics. TiO_2 activity in the visible region together with increase in charge separation can also be enhanced via the creation of a heterojunction with a low bandgap semiconductor (Chandrabose et al. 2021).

Nanotechnology has found wide applications in environmental engineering (Xiao et al. 2020). In recent times, the use of nanocomposites supported with photocatalytic TiO_2 nanoparticles to degrade organic pollutants in dye wastewater is gaining serious attention. The incorporation of nano-TiO_2 helps in stabilizing the nanocomposites due to high vulnerability of their polymer constituent to UV radiation (Nair et al. 2021). Thus, selection of appropriate material with high optical and catalytic activities which also possesses chemical selectivity is imperative. Many supporting materials for nano-TiO_2 such as alumina, silica, porous nickel, zeolites, clays and glass have been reported (Rashed et al. 2017). Table 1 presents previous studies on the use of nanophotocatalyst for the degradation of different dyes in wastewater and aqueous solutions. In our previous studies, calcined rice husk was applied as adsorbent for the removal of brilliant green dye (Popoola et al. 2018; Popoola 2019a, b) from solution due to its high silicate content (Teixeira et al. 2012; Mahross et al. 2016). Also, studies have shown magnetized silicate adsorbents to have excellent hydrophilicity, chemical stability within high pH and silanol groups (Lai et al. 2016; Zhang et al. 2013) which influences their fitness for the removal of pollutants. Not only this, co-precipitation of silicates with magnetite improves its temperature stability, surface area, oxidation strength and superparamagnetic attributes (Popoola 2020; Tahoun et al. 2022). With reference to cited literatures and to the best of authors' knowledge, previous studies rarely considered using SiO_2 nanoparticles synthesized from rice husk and co-precipitated with magnetite and TiO_2 for photocatalytic degradation of dyes in solution. Previous studies have only considered using Ag-TiO_2 nanosheet incorporated in cellulose acetate (Nair and JagadeeshBabu 2017) and TiO_2-AC composites prepared via hydrothermal (Wang et al. 2009), solgel (Xing et al. 2016) and impregnation (Jamil et al. 2012) methods for photocatalytic degradation of different dyes. Not only this, consideration has been given majorly to heavy metals (Popoola 2019b, 2023; Yusuff et al. 2020; Fita et al. 2023).

In this current study, SiO_2 nanoparticles synthesized from rice husk via calcination and a two-stage ball milling process; co-precipitated with magnetite; and supported with TiO_2 via solgel method (TiO_2/mRH-SNP) was used for photocatalytic degradation of methylene blue dye (MBD) from aqueous solution using LED lamp as light source. Factors considered to investigate the photocatalytic degradation efficiency of TiO_2/mRH-SNP were MBD initial concentration, TiO_2 loading, pH and illumination time. Fourier transform infrared, scanning electron microscopy, energy-dispersive X-ray, thermogravimetric analysis, Brunauer–Emmett–Teller, high-resolution transmission electron microscopy and powder X-ray diffractometer were executed to characterize the photocatalyst. The experimental design and optimum point prediction were achieved via Box–Behnken design under response surface of Design-Expert 12. Linearized pseudo-first-order and second-order models were used for the kinetics study.

Materials and methods

Materials

The rice husk was obtained from a small-scale local rice milling industry. Analytical grades of ethanol, titanium (IV) butoxide [$Ti(OC_4H_9)_4$, purity = 98%], methylene blue dye [$C_{16}H_{18}N_3SCI$, molecular weight = 319.85 g/mol, melting point = 100–110 °C], iron (III) chloride [$FeCl_3$] and iron (II) sulfate [$FeSO_4{\cdot}7H_2O$] were used. Sodium hydroxide and hydrochloric acid were used to adjust the pH. All materials bought were used without further modification.

Synthesis of silica nanoparticles from rice husk (RH-SNP)

Thermal treatment, calcination and a two-stage ball milling processes were employed to prepare silica nanoparticles from rice husk (RH). The rice husk was thoroughly washed with water to remove dirt and unwanted materials, sun-dried for 5 days under atmospheric condition and then dried in an oven operated at 100 °C for 5 h. A muffle furnace (Carbolite, ELF11/6B, S/N 21–403,009, UK), operated at 400 ℃ for 2 h, was used to thermally treat the dried RH and disintegrate the organic constituents. The RH was then subjected

Table 1 Previous nanophotocatalysts used for dyes degradation at different process conditions

Nanophotocatalyst	Dyes	Process conditions	Light source	Percentage removed	Reference
TiO_2/mRH-SNP	Methylene blue	DIC = 10 ppm, pH = 6, t = 75 min, TiO_2 loading = 15%	LED lamp	96.89%	Current study
ZnO-SnO_2 nanoparticles	Methylene blue Yellow quinoline Rhodamine B Trypan blue Orange methylene	DIC = 18 mg/L, PD = 200 mg/L, t = 60 min	UV light	76.44% 72.69% 62.43% 77.00% 92.46%	Długosz et al. (2022)
Chitosan–magnetite nanoparticles	Basic Blue 9	PD, 3 mg/L, pH = 7, t = 120 min	UV	99%	Elsayed et al. (2022)
Sawdust/magnetite	Red K-HL	pH = 3.0, PD = 1 g/L	–	99%	Tony (2022)
2-D MoS_2/TiO_2 nanocomposite	Methylene blue Crystal violet Rhodamine B Methyl orange	DIC = 50 mg/L, PD = 0.8 g/L, t = 60 min	UV light	73%	Chandrabose et al. (2021)
TiO_2 nanosheets/cellulose acetate/ethylene vinyl acetate	Congo red dye	DIC 30 ppm, t = 120 min	UV	56%	Nair et al. (2021)
Kaolinite/TiO_2/ZnO	anionic azo dyes	DIC = 100 mg/L, PD = 100 mg/L, pH = 2.5, t = 120 min	Sunlight	98%	Hassan et al. (2020)
$LaFeO_3$/BiOBr	Rhodamine B	DIC = 5 ppm, PD = 0.1 g, t = 30 min	UV	98.2%	Guan et al. (2020)
ZnO/pumice composite	Textile dye effluent	DIC = 3.01 mg/L, PD = 3 g/L, pH = 4.01, t = 45.04 min	Sunlight	90.17%	Yusuff et al. (2020)
TiO_2@NH_2-MIL-88B(Fe)	Methylene blue	pH = 7, DIC = 100 ppm, PD = 200 mg/L, t = 150 min	LED lamp	99%	Li et al. (2018)
ZnO/reduced graphene oxide	–	DIC = 10 mg/L, PD = 0.05 g/L, t = 120 min	Visible light	51%	Ravi et al. (2018)
$PbCrO_4$/TiO_2	Rhodamine B	–	–	–	Abou-Gamra et al. (2017)
TiO_2/sewage sludge-based activated carbon nanocomposites	Methylorange	DIC = 25–100 mg/L, pH = 4–9, t = 30–360 min	UV	94.28%	Rashed et al. (2017)
Electrospun PAN/O-MMT-TiO_2	Methylene blue	DIC = 0.02 g/L, PD = 5 g/L, t = 60 min	UV light	98.66%	Wang et al. (2012)
Electrospun P(3HB)-TiO_2 nanocomposite fibers and films	Malachite green	DIC = 15 mg/L, PD = 4 g/L, t = 120 min	Solar	78%	Sridewi et al. (2011)

DIC dye initial concentration (mg/L); *PD* photocatalyst dosage (g/L); *t* illumination time (min)

to calcination in the same furnace at 800 ℃ and heated for another 2 h.

The silica nanoparticle (SNP) was prepared by dissolving about 50 g of RHA in 50 wt% HCl solution. The mixture was continuously stirred for 4 h till homogeneity. The mixture (white powder of RHA and HCl) was filtered, thoroughly washed with distilled water to obtain neutrality (pH = 7), dried for 4 h at 100 ℃ and stored in a desiccator. A two-stage ball milling process was adopted to reduce the particle size into nanoscale via the use of a planetary ball milling machine. Clustering of particles was prevented, and RH-SNP size was attained by dispersing stored samples in ethanol followed by wet milling at 400 rpm for 5 h. The collected sample was then oven-dried for 18 h at 70 ℃.

Magnetization of RH-SNP

A simple co-precipitation method was used to prepare magnetized RH-SNP (mRH-SNP) composites. Magnetite solution was prepared by mixing $FeSO_4 \cdot 7H_2O$ and $FeCl_3$ in 50 mL of distilled water at a ratio and temperature of 1:2 and 70 ℃, respectively, for 1 h. About 40 g of RH-SNP and 50 mL of 1 M citric acid were added to the mixture, mixed thoroughly via magnetic stirrer and heated on a mantle to

100 ℃ for 1 h. The precipitate was then washed till neutrality using distilled water and dried under vacuum in an oven at 100 ℃ for 2 h.

Synthesis of TiO_2/mRH-SNP as photocatalyst

Nanoparticle of TiO_2 was deposited onto mRH-SNP surface by solgel method. This was achieved by dissolving 50 mL of $Ti(OC_4H_9)_4$ in 100 mL of ethanol in beaker and stirred mechanically at room temperature for 1 h. Fifty mL of 1 M nitric acid was added to the mixture and rigorously stirred to obtain a clear transparent sol. Impregnation of mRH-SNP in the TiO_2 solution was executed at specified loading, and the product was placed on a heating mantle at 100 ℃ and then oven-dried at 130 ℃ for 12 h to completely evaporate the ethanol present in the mixture and obtain TiO_2/mRH-SNP as photocatalyst.

Preparation of MBD solution

A stock solution of 1000 ppm was prepared at room temperature by dissolving 1 g of MBD in 1 L of distilled water in 1000-mL round bottom flask. MBD solutions of different initial concentrations were prepared via successive dilution of the stock solution for the batch photodegradation process.

Batch photodegradation process

The photodegradation capacity of TiO_2/mRH-SNP was tested on MBD in aqueous solution. Different concentrations of MBD were prepared, and 100 mL of each was placed in a glass beaker as required. The initial solution pH was adjusted, as required, by adding 1 M NaOH and/or diluted HCl solutions using a digital pH meter (OAKION, Eutech Instruments, Singapore). TiO_2/mRH-SNP with different loading (as suggested by Box–Behnken design) was dispersed in the MBD solution and was continuously stirred at 120 rpm using a magnetic stirrer in the absence of light for 60 min at room temperature to attain adsorption–desorption equilibrium. The photocatalytic process of the samples was conducted by placing LED lamp as illumination source at a distance of 25 cm from the liquid surface to initiate the oxidation reaction. Samples were filtered using Whatman filter paper, and MBD concentration was determined using UV–visible spectrophotometer (Spectrumlab 752 s) at maximum wavelength of 664 nm. The residue is the photocatalyst, wrapped with aluminum foil and kept in a desiccator for further laboratory analysis. The percentage of MBD photodegraded (PMD) and adsorption capacity (q_e) of TiO_2/mRH-SNP are determined using Eqs. (1) and (2), respectively.

$$\mathrm{PMD} = \frac{\left(C_i - C_f\right)}{C_i} \times 100\% \tag{1}$$

$$q_e = \frac{\left(C_i - C_f\right)}{W} V \tag{2}$$

where C_i and C_f = initial and final concentration of MBD (ppm) before and after illumination, V = volume of solution (mL) and W = weight of photocatalyst (mg).

Experimental design

Box–Behnken design (BBD) under response surface of Design-Expert 12 was used for the experimental design and optimum point prediction of MBD photocatalytic degradation using TiO_2/mRH-SNP. Table 2 presents the factor coding and ranges of the original variables. Equation (3) describes the second-order polynomial quadratic model representing the photocatalytic degradation process. The model response is the percentage of MBD photodegraded in solution (PMD), and 29-run experiments were randomly designed as stated in Table 4 with 5 center points per block on the Box–Behnken design. ANOVA was used to affirm the developed model's genuity and fitness for future prediction.

$$\mathrm{PMD}(\%) = \beta_o + \sum \beta_o \xi_i + \sum \beta_{\mathrm{ii}} \xi_i^2 + \sum \sum \beta_{\mathrm{ij}} \xi_i \xi_j \tag{3}$$

Characterization

Fourier transform infrared spectrophotometer (Nicolet iS10), scanning electron microscope (SEM/EDX-JEOL-JSM 7600F), energy-dispersive X-ray, TGA–DSC analyzer (PerkinElmer; analysis condition: heating rate = 30 °C min^{-1}, N_2 carrier flow rate = 20 mL min^{-1} and temperature range = 30—800 °C) and Brunauer–Emmett–Teller method (Nova 11.03A, USA version) were, respectively, used to investigate the functional groups, structural morphology, elemental weight%, thermal decomposition profile and textural properties of raw rice husk, prepared and used TiO_2/mRH-SNP for MBD degradation. High-resolution transmission electron microscopy (HRTEM, JEOL-JSM CM178) was utilized to examine the morphological structure and

Table 2 Factor coding and variable ranges for MBD photodegradation using Box–Behnken design

Independent variables	Factor	Unit	Low level (−1)	Center point (0)	High level (+1)
MBD initial concentration	ξ_1	(ppm)	10	30	50
TiO_2 loading	ξ_2	(%)	5	15	25
Solution pH	ξ_3	–	2	6	10
Illumination time	ξ_4	(min)	15	45	75

particle size of as-prepared TiO_2/mRH-SNP. The crystal structure via phase composition of mRH-SNP and as-prepared TiO_2/mRH-SNP was investigated by powder X-ray diffractometer (Rigaku D/Max-III, Tokyo, Japan) using Cu K α radiation (0.154 Å).

TiO_2/mRH-SNP regeneration and reusability

The ability of TiO_2/mRH-SNP to be used repeatedly for MBD degradation from solution was tested. The used catalyst was regenerated from the mixture after each reaction by filtration. Distilled water was used to thoroughly wash the spent catalyst and recalcined for 60 min at 400 °C in a muffle furnace. The percentage of MBD degraded was measured for each photocatalytic process after repeating the catalyst regeneration–washing–calcination process for five consecutive periods under optimal process conditions.

Results and discussions

TiO_2/mRH-SNP characterization

Fourier transform infrared

As shown in Fig. 1, peaks observed at 3444.98 cm^{-1}, 3018.69 cm^{-1}, 2916.47 cm^{-1}, 2000.25 cm^{-1} and 1653.05 cm^{-1} in the raw rice husk, prepared TiO_2/mRH-SNP and used TiO_2/mRH-SNP spectra could be ascribed to strong O–H stretching vibration, weak O–H stretching vibration, strong C–H stretching, strong N=C=S stretching and strong C=O stretching, respectively (Xing et al. 2016). Peaks formed at 2519.12 cm^{-1}, 1803.50 cm^{-1}, 877.64 cm^{-1} and 713.69 cm^{-1} on raw rice husk spectrum disappeared after magnetization and addition of TiO_2 to the silica nanoparticles from rice husk. The prepared TiO_2/mRH-SNP spectrum shows new peaks around 2350 cm^{-1}, 1600 cm^{-1}, 970 cm^{-1} and 495 cm^{-1} which could be ascribed to the removal of weak S–H stretching, formation of Fe–O–Ti bond, formation of Si–OH bond and formation of Si–O–Fe bond, respectively (Abbas et al. 2014). This resulted from the reaction between iron in the magnetite solution and titanium in the photocatalyst with the silicate present in the raw rice husk (Du et al. 2006). Also, peak formed at 464.86 cm^{-1} on prepared TiO_2/mRH-SNP disappeared after MBD photodegradation which affirms the occurrence of adsorption process (Xiao et al. 2020).

Surface morphology and particle size verification

The scanning electron images of raw rice husk, prepared TiO_2/mRH-SNP and used TiO_2/mRH-SNP are presented in Fig. 2a–c, respectively. The micrograph of raw rice husk (Fig. 2a) shows a flake-like and unevenly distributed morphology with very few pore openings. The micrograph of prepared TiO_2/mRH-SNP (Fig. 2b) revealed wide pore openings covered with granule-like shaped titanium oxide on the surface of the particle. Figure 2c representing the SEM

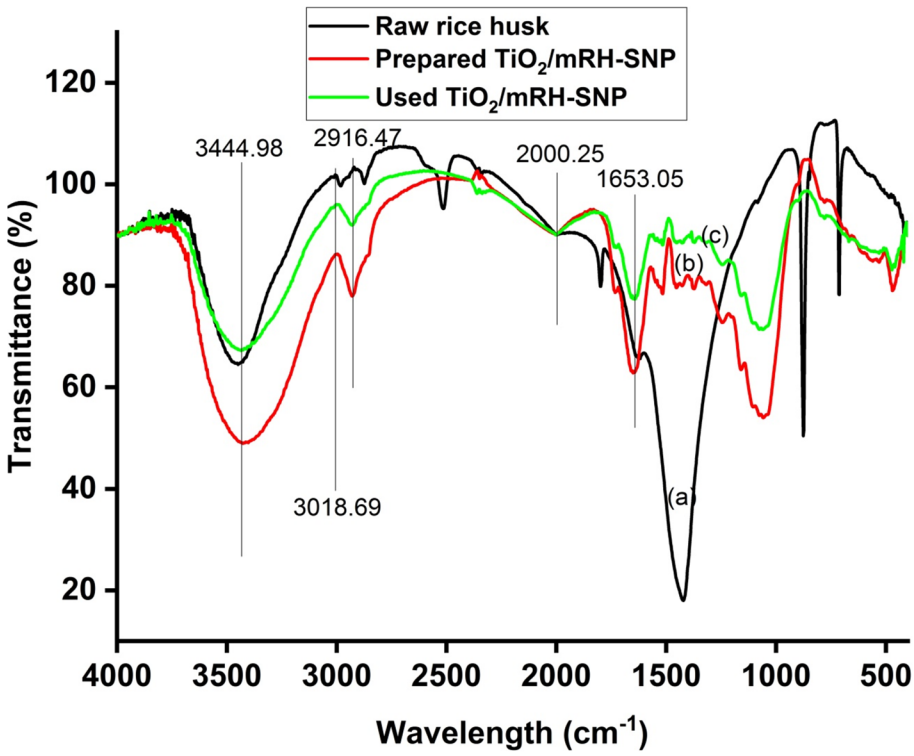

Fig. 1 FTIR spectra of raw rice husk, prepared TiO_2/mRH-SNP and used TiO_2/mRH-SNP

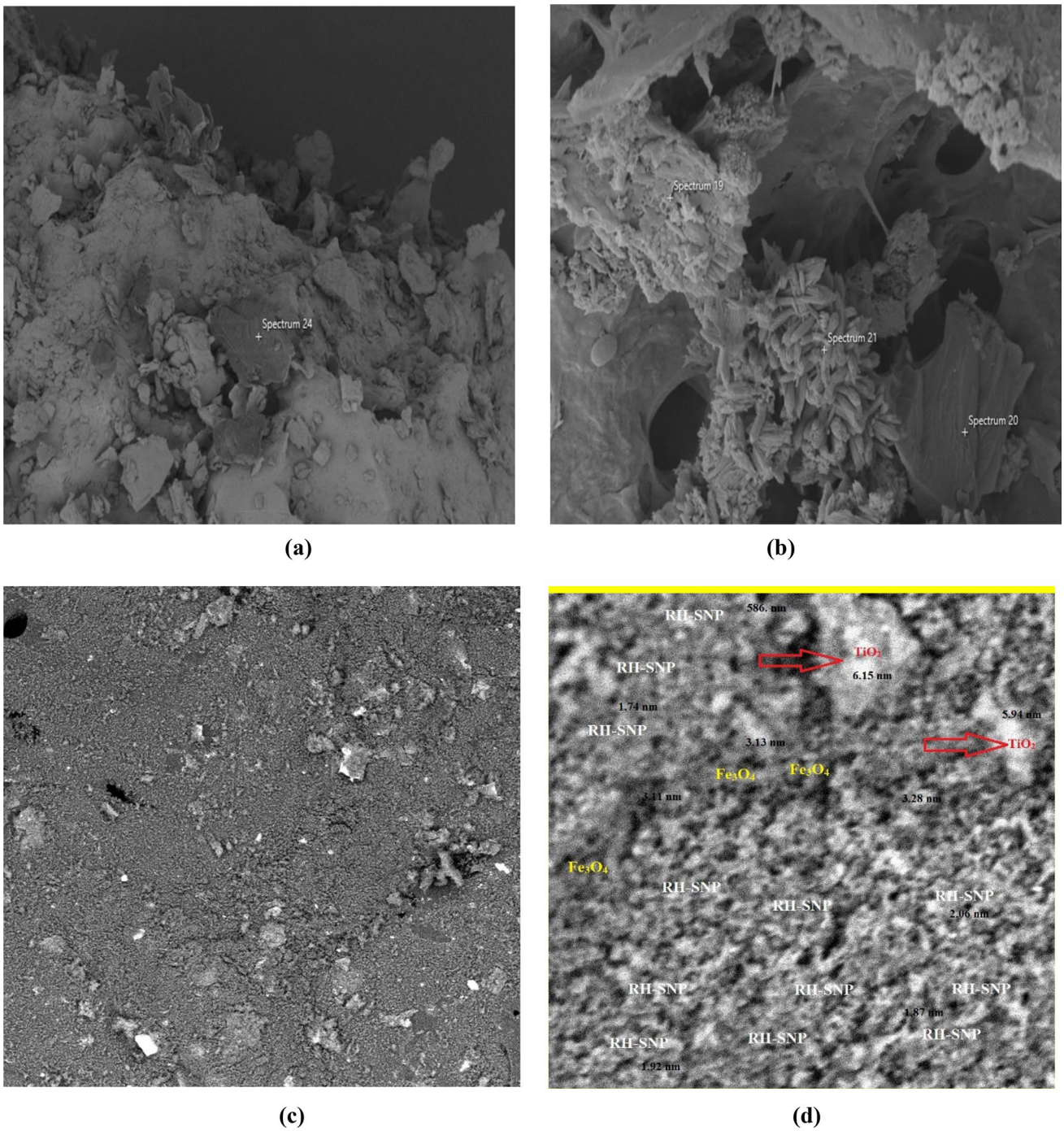

Fig. 2 SEM micrograph of **a** raw rice husk **b** as-prepared TiO_2/mRH-SNP and **c** used TiO_2/mRH-SNP; and **d** HRTEM of b

image of used TiO_2/mRH-SNP reveals a slightly smooth surface with little pores resulting from wide pore coverage by MBD after the photocatalytic degradation. Figure 2d presents the high-resolution transmission electron microscopy (HRTEM) image of as-prepared TiO_2/mRH-SNP, and some dark areas (densely in appearance) were observed which resulted from the agglomeration of magnetic crystalline particles of Fe_2O_3 with mean diameter of approximately 3.3 nm. These were surrounded by relatively white particles of RH-SNP having an average diameter of about 1.85 nm. To add up, agglomeration of brighter particles of TiO_2, surrounded by the dark dense and relatively white particles, with average diameter of approximately 6.0 nm in two major regions was noticed.

Energy-dispersive X-ray

The EDX analysis result of raw rice husk (Fig. 3a) discloses presence of carbon (45.1 wt%), oxygen (43.6 wt%) and silicon (11.3 wt%). This could be attributed to the presence of carbon and oxygen in the lignin, cellulose and hemicellulose content of the rice husk. The weight percent of silicon recorded could be attributed to the high silicate content of rice husk (Mahross et al. 2016). The EDX result of prepared TiO_2/mRH-SNP (Fig. 3b) revealed reduction in the percentage of carbon and silicon to 25.3 wt% and 6.7 wt% as a result of decomposition of the carbon content in the raw rice husk during the synthesis of silica nanoparticles via thermal treatment and calcination processes. The presence of 64.7 wt% for oxygen resulted from its addition from the titanium oxide compound used as photocatalyst. Also, the result revealed the presence of iron (1.4 wt%) and titanium (0.2 wt%) at different peaks due to magnetization and photocatalysis of the synthesized silica nanoparticles. However, the carbon wt% in the used TiO_2/mRH-SNP increased to 77.0 wt% (Fig. 3c) after the photodegradation. This resulted from the adsorption of carbon content of the MBD ($C_{16}H_{18}N_3SCI$) by the photocatalyst. The absence of iron and silicon after MBD removal could be attributed to their active involvement in enhancing the photodegradation process.

Thermogravimetric study

Figure 4 shows the weight loss behavior of raw rice husk, prepared TiO_2/mRH-SNP and used TiO_2/mRH-SNP at different temperatures. Each of the samples exhibited different thermal decomposition trend. Three stages of decomposition were observed, and loss of weight was noticed between 0 and 93 °C (due to water molecules removal), 93 and 380 °C (as a result of lignin decomposition present in the rice husk) and 340 and 750 °C (resulting from cellulose and hemicellulose removal) for the samples (Thushari and Babel 2020). The raw rice husk and prepared TiO_2/mRH-SNP exhibited constant weight loss after 575 °C and 605 °C, respectively. This shows that the magnetization and addition of TiO_2 to the raw rice bran improved the thermal stability behavior of prepared TiO_2/mRH-SNP. Also, the prepared TiO_2/mRH-SNP recorded the lowest weight loss out of the examined samples.

Brunauer–Emmett–Teller

Table 3 presents the BET textural analysis results of RH-SNP, mRH-SNP and TiO_2/mRH-SNP together with the photocatalysts used in previous studies. Total pore volume, surface area and average pore diameter of 0.017, 0.032 and 0.075 cm^3/g; 38.11, 54.92 and 144.06 m^2/g; and 1.832, 3.027 and 5.886 nm were recorded for RH-SNP, mRH-SNP and TiO_2/mRH-SNP, respectively. TiO_2/mRH-SNP exhibited highest total pore volume, surface area and average pore diameter which could be attributed to the magnetization of RH-SNP and addition of titanium oxide to mRH-SNP which in return enhances the photodegradation of MBD from aqueous solution.

Powder X-Ray difractometer

Figure 5 presents the XRD pattern of mRH-SNP and as-prepared TiO_2/mRH-SNP studied at 2θ value between 0 and 70°, Cu K α radiation (0.154 Å). The XRD data revealed mRH-SNP to be crystalline in nature with the following phases: quartz [tetrahedral, 2θ (20°, 26°, 35°, 50° and 60°)], magnetite [2θ (23°, 45° and 55°)] and silicon oxide [hexagonal, 2θ (32°, 36°, 42° and 68°)] as presented in Fig. 5a. The major crystalline phases of as-prepared TiO_2/mRH-SNP as shown in Fig. 5b include quartz [tetrahedral, 2θ (20°, 26°, 33°, 45° and 56°)], magnetite [2θ (25°, 40°, 48° and 60°)], silicon oxide [monoclinic, 2θ (34°, 54° and 66°)] and titanium oxide [monoclinic, 2θ (2°, 6°, 10°, 12°, 16° and 18°)]. The average crystalline size of mRH-SNP and as-prepared TiO2/mRH-SNP as revealed by BET is 3.027 nm and 5.886 nm, respectively (Table 3).

Box–Behnken design, model fitness and statistical analysis

Table 4 presents the experimental and predicted percentage of MBD photodegraded in solution (responses) at different process parameters (variables) generated by Box–Behnken design of Design-Expert software. At MBD initial concentration, TiO_2 loading, pH and illumination time of 10 ppm, 15%, 6 and 75 min, respectively, and 96.51% of MBD was photodegraded. This was observed to be the maximum value for the percentage of MBD removed from solution. The results obtained were used to develop a mathematical model which relates the independent process parameters with percentage of MBD photodegraded for future prediction. At the observed maximum conditions, 97.16% of MBD was predicted to be photodegraded using TiO_2/mRH-SNP by the developed model represented as Eq. (4).

$$\begin{aligned}\text{PMD}\ (\%) = {} & +\ 71.56 - 9.29\,\xi_1 + 6.71\,\xi_2 - 2.34\,\xi_3 \\ & + 7.34\,\xi_4 - 1.32\,\xi_1\xi_2 + 1.66\,\xi_1\xi_3 - 4.91\,\xi_1\xi_4 \\ & - 1.29\,\xi_2\xi_3 + 0.63\,\xi_2\xi_4 + 0.6425\,\xi_3\xi_4 \\ & +\ 1.21\,\xi_1^2 + 1.26\,\xi_2^2 + 0.7347\,\xi_3^2 - 1.14\,\xi_4^2 \end{aligned} \quad (4)$$

Other predicted values of PMD by Eq. (4) are presented in Table 4. In general, the experimental and predicted values of PMD exhibited excellent correlations as reported from

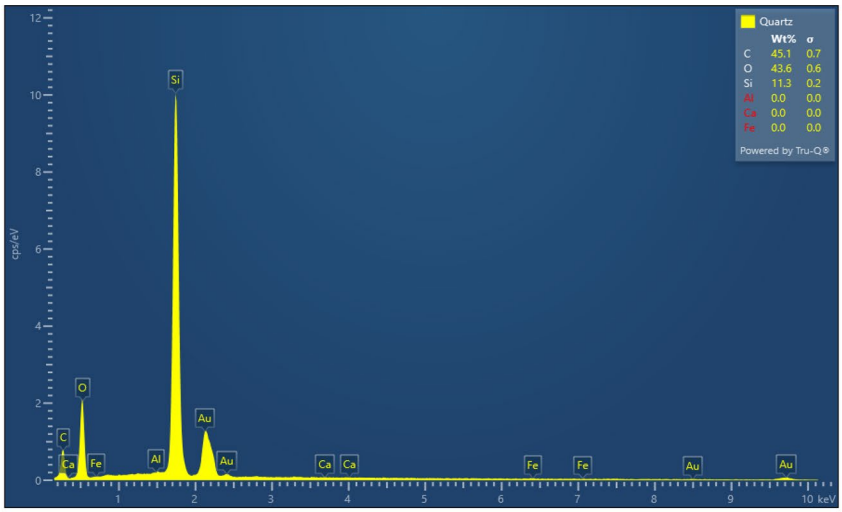

(a)

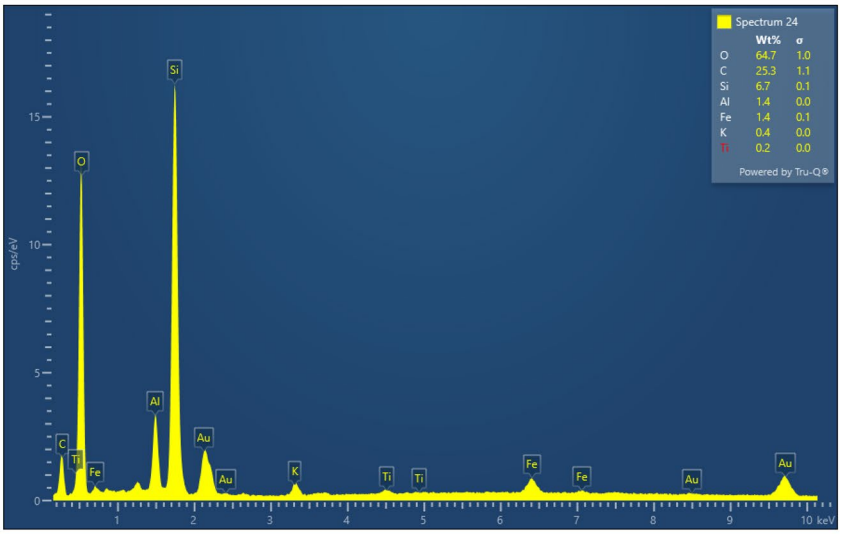

(b)

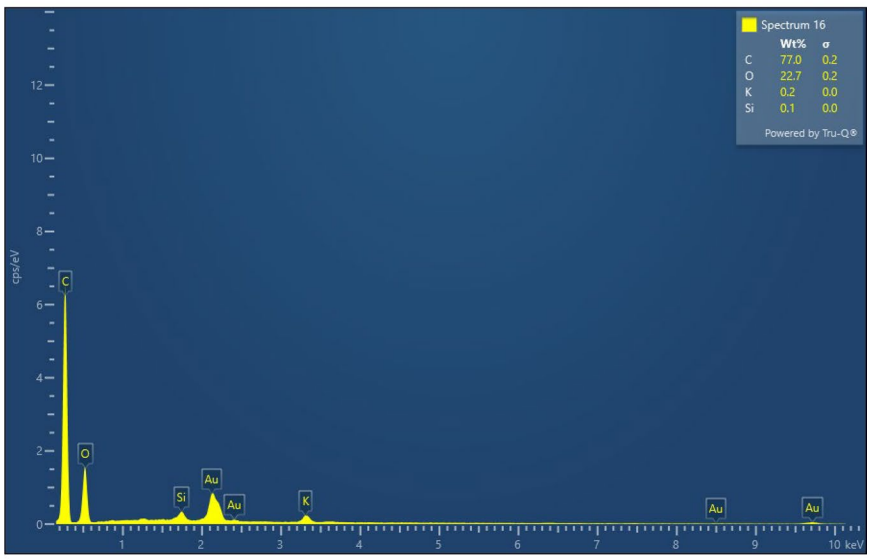

(c)

Fig. 3 Energy dispersive X-ray of **a** raw rice husk **b** prepared TiO_2/mRH-SNP and **c** used TiO_2/mRH-SNP

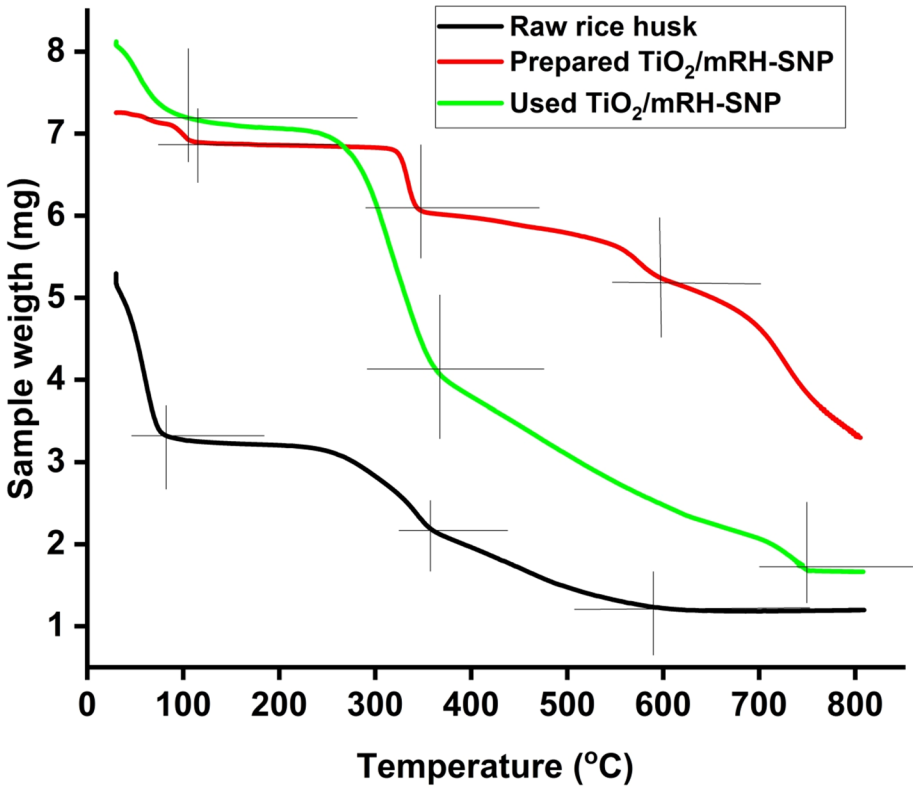

Fig. 4 Thermogravimetric analysis of **a** raw rice husk **b** prepared TiO_2/mRH-SNP and **c** used TiO_2/mRH-SNP

Table 3 Brunauer–Emmett–Teller result of different photocatalysts used in previous and current studies

Photocatalyst	Total pore volume (cm^3/g)	Surface area (m^2/g)	Average pore diameter (nm)	References
Nanometer oxides SnO_2	–	16.57	20.7	Yuan and Xu (2010)
Merck TiO_2	–	6.4	–	Nainani et al. (2012)
Degussa P25 TiO_2	–	50.00	–	Nainani et al. (2012)
Ag-TiO_2	–	140.00	–	Nainani et al. (2012)
Prepared TiO_2	–	150.00	–	Nainani et al. (2012)
Anatase TiO_2 nanoparticles	–	186.25	–	Wei et al. (2013)
Fe_3O_4	0.14	111.0	5.0	Dagher et al. (2018)
Fe_3O_4@TiO_2	0.13	76.0	6.9	Dagher et al. (2018)
Fe_3O_4@SiO_2	0.42	138.0	10.2	Dagher et al. (2018)
ZnO-pumice composite	0.0228	122.81	29.80	Yusuff et al. (2020)
Magnetic Fe_3O_4@SiO_2 /TiO_2	–	181	–	Bielan et al. (2020)
Cu–Fe/TiO_2	–	2.10	–	Khan et al. (2021)
ZnO-coal fly ash400	0.230	58.8	80.0	Yusuff et al. (2022)
CuO@TiO_2	3.12×10^{-2}	19.0	6.08	Hamad et al. (2022)
Pure ZnO	0.010	22.27	1.453	Nnodim et al. (2022)
Green N-ZnO	0.055	113.3	2.118	Nnodim et al. (2022)
$MnCo_2O_4$	–	155.0	–	Jiménez-Miramontes et al. (2022)
RH-SNP	0.017	38.11	1.832	Current study
mRH-SNP	0.032	54.92	3.027	Current study
TiO_2/mRH-SNP	0.075	144.06	5.886	Current study

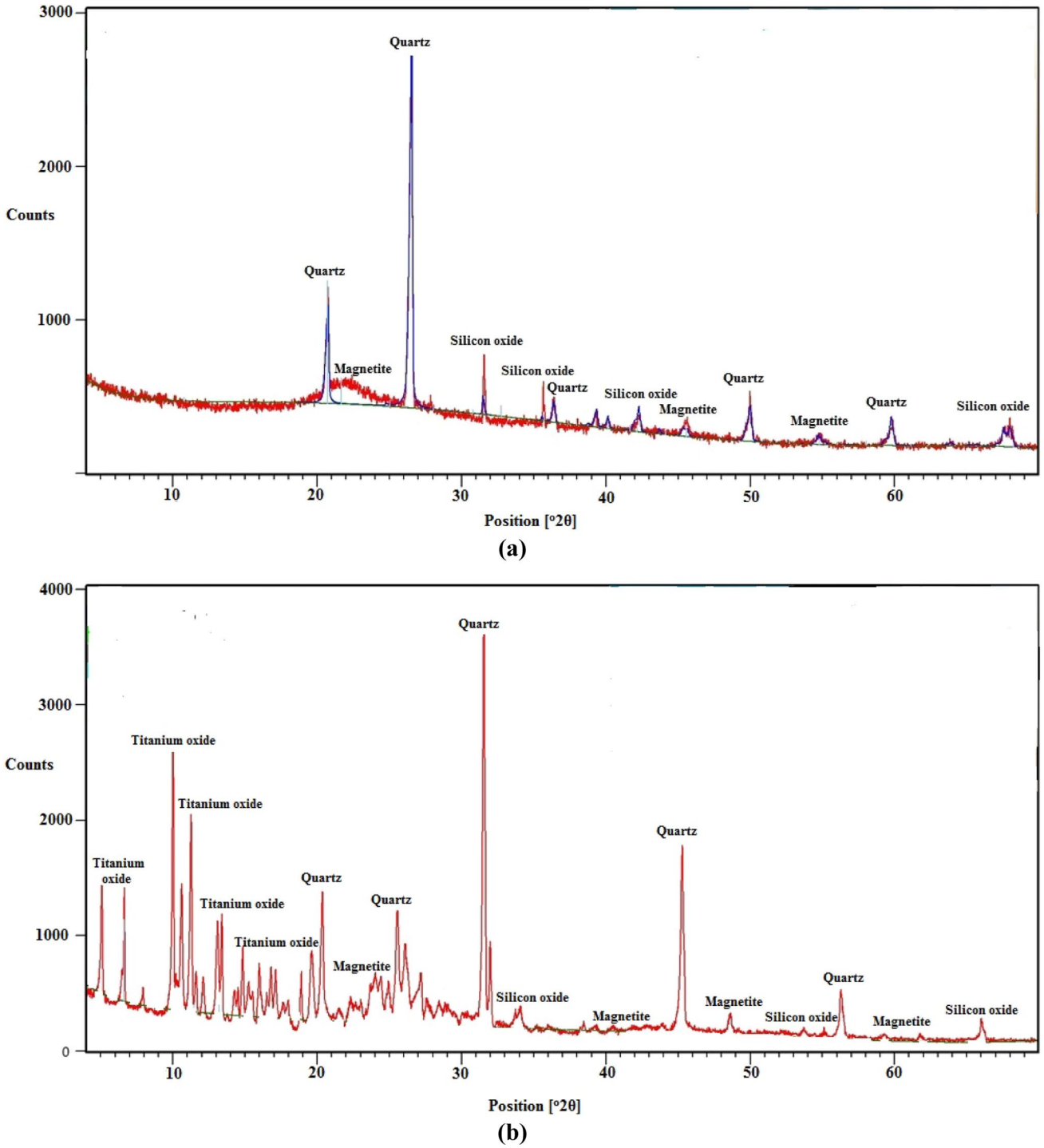

Fig. 5 XRD pattern of **a** mRH-SNP and **b** prepared TiO_2/mRH-SNP

the correlation coefficient (R^2-value) of 0.9569 obtained from the plot of PMD_{exp} versus PMD_{pred} values presented in Fig. 6. This suggests high degree of model fitness for future prediction. The model could effectively explain 95.69% of the process parameters investigated in the study for PMD prediction while only 4.31% of the variables could not be explained by the developed model.

Table 5 presents the analysis of variance (ANOVA) results obtained to substantiate the model fitness and significance. The F-value (a ratio of model mean square to residual error) and p-value were used as the tools for

Table 4 Box–Behnken design parameters, experimental and predicted responses

Run	MBD initial concentration	TiO_2 loading	pH	Illumination time	PMD_{exp}	PMB_{pred}
	ppm	%		Min	%	%
1	30	5	10	45	63.79	65.8
2	50	5	6	45	60.11	59.35
3	50	15	2	45	65.45	64.89
4	50	15	6	15	61.08	59.90
5	10	15	2	45	89.91	86.78
6	30	5	6	15	61.53	58.25
7	30	25	2	45	86.42	83.89
8	50	15	10	45	61.73	63.54
9	10	15	10	45	79.54	78.79
10	50	25	6	45	67.84	70.13
11	30	15	10	75	76.88	76.80
12	10	5	6	45	75.74	75.29
13	30	15	6	45	72.98	71.56
14	30	25	6	15	70.34	70.41
15	30	15	6	45	69.7	71.56
16	10	15	6	75	96.51	97.16
17	10	15	6	15	67.57	68.65
18	30	15	6	45	70.04	71.56
19	30	5	6	75	73.06	71.68
20	30	5	2	45	64.03	67.89
21	30	25	6	75	84.39	86.35
22	30	15	6	45	73.41	71.56
23	10	25	6	45	88.74	91.33
24	30	15	6	45	71.66	71.56
25	30	25	10	45	81.01	76.63
26	30	15	2	75	79.74	80.19
27	50	15	6	75	66.38	64.77
28	30	15	10	15	59.44	60.83
29	30	15	2	15	64.87	66.78

the ANOVA. A good model predictor of experimental values exhibits *F*-value higher than *F*-distribution value and a *p*-value less than 0.05. The ANOVA result revealed model *F*-value of 22.18 (higher than the *F*-distribution value of 2.57) and a *p*-value lesser than 0.0001 suggesting the model accuracy and significance to the study. Also, the examined parameters are significant to the model and contributed to the MBD photodegradation because their *F*-value is less than 0.05.

The percentage contribution of each of the process parameters to the percentage of MBD photodegraded from solution (response) was determined by Eq. (5), and the result is presented in Fig. 7. The result revealed high significance of MBD initial concentration, TiO_2 loading, pH, illumination time and MBD initial concentration–illumination time with percentage contribution of 42.35%, 22.09%, 2.68%, 26.49% and 3.95%, respectively.

$$\text{Percentage contribution} = \left[\frac{SS_i}{\sum SS_i}\right] \times 100\% (i \neq 0) \quad (5)$$

such that SS_i = Sum of square of significant parameter.

3D response surface plots of process parameters effect

The combinatory effect of TiO_2 loading and MBD initial concentration on PMD at solution pH and illumination time of 6 and 45 min, respectively, is shown in Fig. 8a. PMD increases with increase in TiO_2 loading but decrease in

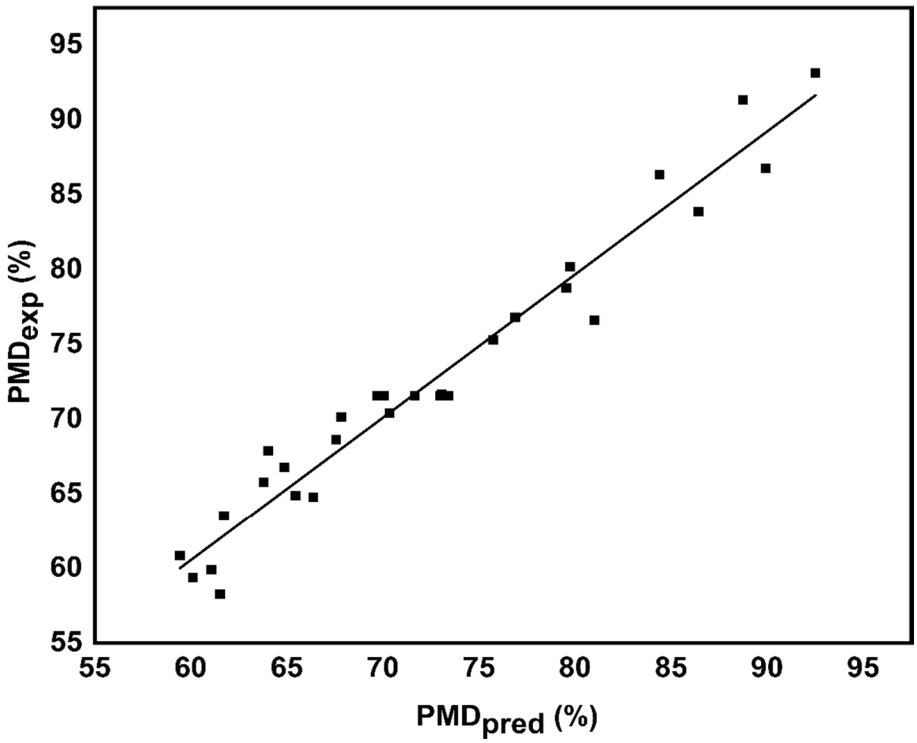

Fig. 6 A plot of PMD_{exp} versus PMD_{pred}

Table 5 ANOVA results

Source	Sum of squares	df	Mean square	*F*-value	*p*-value	
Model	2446.38	14	174.74	22.18	< 0.0001	Significant
MBD initial concentration	1034.53	1	1034.53	131.3	< 0.0001	
TiO_2 loading	539.75	1	539.75	68.5	< 0.0001	
pH	65.47	1	65.47	8.31	0.012	
Illumination time	647.24	1	647.24	82.15	< 0.0001	
$\xi_1\xi_2$	6.94	1	6.94	0.8812	0.3638	
$\xi_1\xi_3$	11.06	1	11.06	1.4	0.2559	
$\xi_1\xi_4$	96.43	1	96.43	12.24	0.0035	
$\xi_2\xi_3$	6.68	1	6.68	0.8481	0.3727	
$\xi_2\xi_4$	1.59	1	1.59	0.2015	0.6604	
$\xi_3\xi_4$	1.65	1	1.65	0.2096	0.6541	
ξ_1^2	9.47	1	9.47	1.2	0.2914	
ξ_2^2	10.27	1	10.27	1.3	0.2727	
ξ_3^2	3.5	1	3.5	0.4444	0.5158	
ξ_4^2	8.47	1	8.47	1.08	0.3174	
Residual	110.31	14	7.88			
Lack of fit	99.09	10	9.91	3.53	0.1176	Not significant
Pure error	11.22	4	2.8			
Cor total	2556.69	28				

MBD initial concentration. This observation could be attributed to increase in the absorption of light photon by MBD molecules resulting from increase in the active sites due to increase in catalyst loading which in return increases the PMD. Also, increase in the initial concentration of MBD causes the blockage of the catalyst active sites by the dye. Thus, reduction in MBD initial concentration is a favorable condition. Figure 8b presents the combinatory effect of pH and MBD initial concentration on PMD at TiO_2 loading and illumination time of 15% and 45 min, respectively. The PMD slightly decreases as solution pH increases from 2 to 10 signifying low contribution of solution pH. At low pH, the

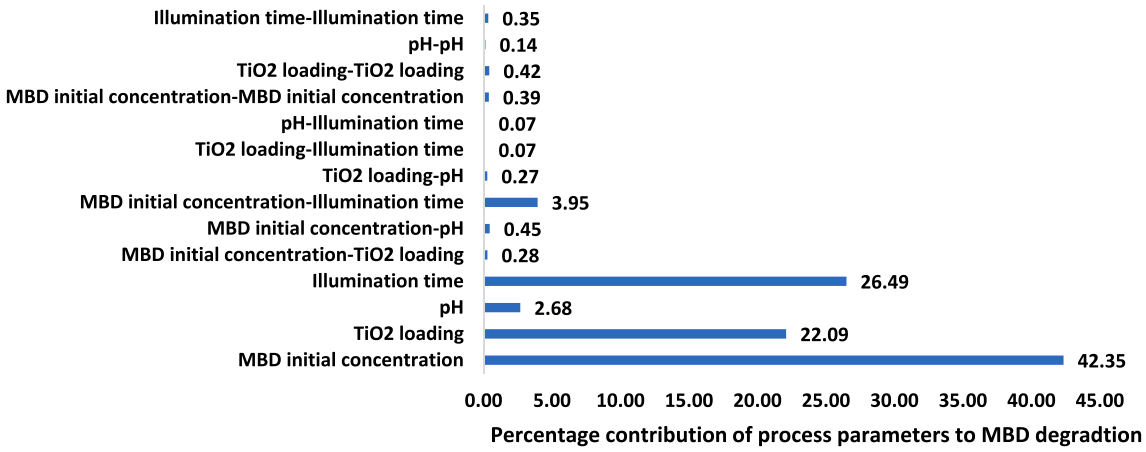

Fig. 7 Bar chart of process parameters effect

amount of MBD adsorbed onto TiO_2/mRH-SNP increased as a result of electrostatic forces of attraction between OH^- on adsorbent surface and H^+ in solution. The interaction effect between MBD initial concentration and illumination time (Fig. 8c) also displayed increase in PMD with increase in illumination time but decrease in MBD initial concentration. This could be attributed to increase in the contact time between molecules of TiO_2/mRH-SNP and MBD which enhances MBD degradation from solution. The combinatory effects of TiO_2 loading and pH (Fig. 8d) and pH and illumination time (Fig. 8f) revealed pH is insignificant because the PMD remains relatively constant as the pH was increased but increases with the increase in TiO_2 loading and illumination time. This is in support of the result presented in Fig. 7 where percentage contribution of pH to PMD was relatively low. The result presented in Fig. 8e shows high significance of TiO_2 loading and illumination time on PMD. It increases with the increase in the values of both parameters.

Optimum point for MBD photodegradation

The optimum predicted condition by BBD was observed at MBD initial concentration, TiO_2 loading, pH and illumination time of 10 ppm, 15%, 6 and 75 min, respectively. At this condition, the predicted PMD was 97.66% (Table 6). Further laboratory experiment was conducted at this condition, and 96.89% of MBD was photodegraded from solution. This affirms the effectiveness of TiO_2/mRH-SNP in degrading MBD from solution. Comparison of TiO_2/mRH-SNP with previously used adsorbents for various dyes removal from solution via photocatalytic degradation is presented in Table 1.

Kinetics study

Linearized pseudo-first-order and pseudo-second-order kinetic models stated, respectively, as Eqs. (6) and (7) were used to analyze the kinetics of MBD photodegradation using TiO_2/mRH-SNP. The kinetic parameters k_1 and k_2 were determined via plots of ln $(q_t\text{-}q_e)$ against t (Fig. 9a) and t/q_t against t (Fig. 9b), respectively. The correlation coefficient R^2 for each plot and the kinetic parameters are presented in Table 7. The result revealed experimental data to be well-fitted into pseudo-second-order kinetic model with R^2 of 0.999.

$$\mathrm{In}\left(q_e - q_t\right) = \mathrm{Inq}_e - k_1 t \tag{6}$$

$$\frac{t}{q_t} = \frac{1}{k_2 q_e^2} + \frac{t}{q_e} \tag{7}$$

where q_e = equilibrium experimental adsorption capacity (mg g^{-1}), q_t = adsorption capacity at illumination time t (mg g^{-1}), k_1 = pseudo-first-order rate constant (min^{-1}) and k_2 = pseudo-second-order rate constant (g mg^{-1} min^{-1}).

Temperature effect on MBD photodegradation using TiO_2/mRH-SNP

The reaction temperature is an essential factor which should be considered to know how a photocatalyst behave toward the degradation of a pollutant in solution. In this study, the degradation efficiency of TiO_2/mRH-SNP with TiO_2 loading of 15% was investigated between 30 and 70 °C for MBD solution with initial concentration of 10 ppm at a pH of 6 for an illumination period of 75 min. The result (Fig. 10) revealed a steady increase in the percentage of MBD degraded from 81.06 to 91.86% between 30 °C and 50 °C after which the percentage degraded reduced to 83.28%

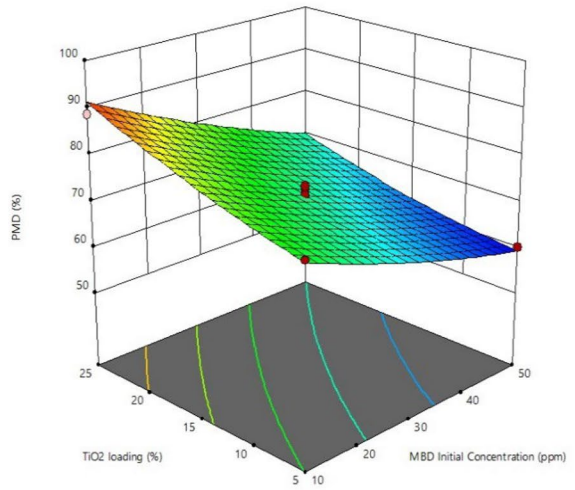
PMD (%)
100
90
80
70
60
50
25
20
15
10
5
TiO2 loading (%)
10
20
30
40
50
MBD Initial Concentration (ppm)

(a)

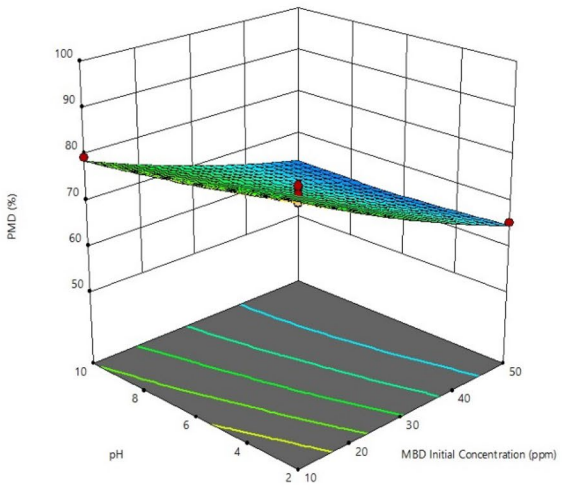
PMD (%)
100
90
80
70
60
50
10
8
6
4
2
pH
10
20
30
40
50
MBD Initial Concentration (ppm)

(b)

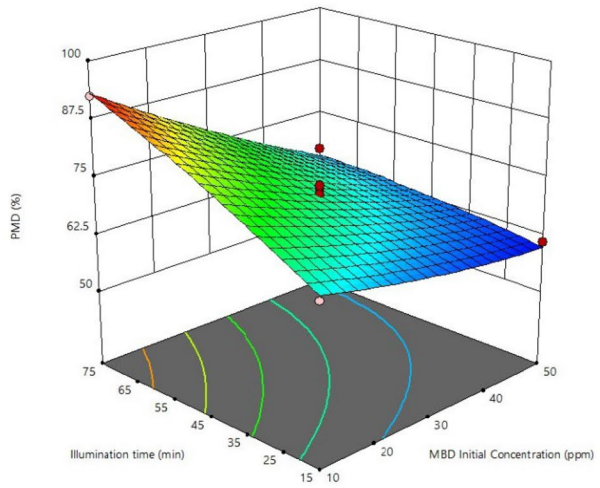
PMD (%)
100
87.5
75
62.5
50
75
65
55
45
35
25
15
Illumination time (min)
10
20
30
40
50
MBD Initial Concentration (ppm)

(c)

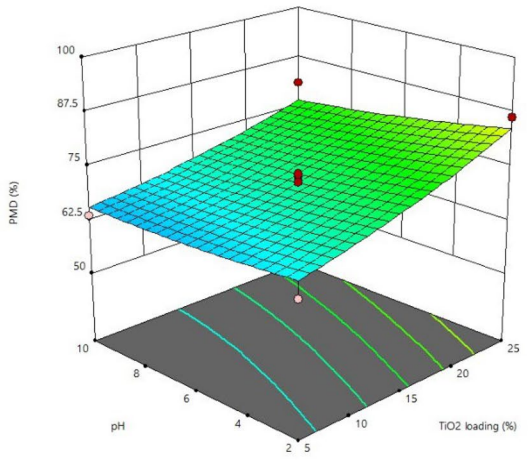
PMD (%)
100
87.5
75
62.5
50
10
8
6
4
2
pH
5
10
15
20
25
TiO2 loading (%)

(d)

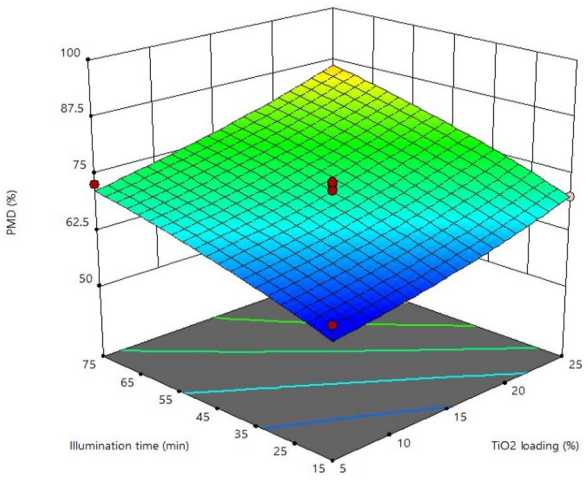
PMD (%)
100
87.5
75
62.5
50
75
65
55
45
35
25
15
Illumination time (min)
5
10
15
20
25
TiO2 loading (%)

(e)

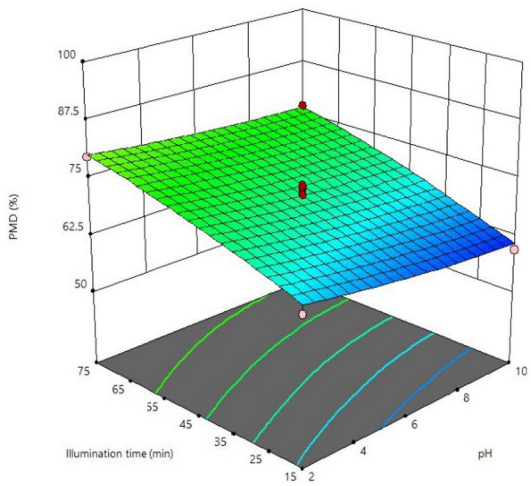
PMD (%)
100
87.5
75
62.5
50
75
65
55
45
35
25
15
Illumination time (min)
2
4
6
8
10
pH

(f)

◂**Fig. 8** 3D response surface of **a** MBD initial concentration (ppm) and TiO_2 loading (%) **b** MBD initial concentration (ppm) and pH **c** MBD initial concentration (ppm) and illumination time (min) **d** TiO_2 loading (%) and pH **e** TiO_2 loading (%) and illumination time (min), and **f** pH and illumination time (min) on MBD photocatalytic degradation

Table 6 Predicted and experimental values of PMD at optimum predicted point by BBD

MBD initial concentration	TiO_2 loading	pH	Illumination time	PMD_{pred}	PMB_{exp}
ppm	%		min	%	%
10	15	6	75	97.66	96.89

between 50 °C and 70 °C. The increase in the number of free radicals produced in solution as a result of more bubbles formation (at a temperature below 50 °C) might be responsible for the steady increase in the percentage of MBD degraded. Under this condition, the rate of MBD molecules oxidation at TiO_2/mRH-SNP interface is improved. Above 50 °C, the oxygen saturation level was reduced and this hindered the formation of reactive superoxide radicals. This is an essential mechanism step needed to capture photogenerated electrons in order to improve $\cdot O_2^-$ formation, and thus, a reduction in the percentage of MBD degraded was noticed (Herrmann 1999). The result obtained was similar to the study conducted by Sodeinde et al. (2022) which applied reduced graphene oxide-ZnO as photocatalyst to degrade chloramphenicol in solution using UV light.

Table 7 Kinetic study of MBD photodegradation using TiO_2/mRH-SNP

Pseudo-first-order		Pseudo-second-order	
$k_1 \times 10^{-2}$	R^2	$k_2 \times 10^{-4}$	R^2
7.67	0.917	2.40	0.999

Reusability of TiO_2/mRH-SNP

Figure 11 presents the reusability of TiO_2/mRH-SNP for MBD photodegradation at the optimum predicted point after five consecutive cycles. The photodegradation efficiency decreases from 91.89 to 57.60%. This resulted from the active sites blockage on TiO_2/mRH-SNP surface by the adsorbed dye molecules which in return reduce the rate of MBD degradation. The adsorbed dye molecules increase the active radicals ($\cdot OH$ and $\cdot O_2^-$) needed for MBD degradation. At given illumination time and TiO_2/mRH-SNP dosage, the active radicals formed on the regenerated catalyst surface remain constant as the reaction cycle continues. Thus, the percentage of MBD degraded reduces as the catalyst was reused due to insufficient $\cdot OH$ radicals. Table 8 compares the reusability and stability of some previous photocatalysts used for degradation of pollutants (majorly dyes) with present study.

Proposed photocatalysis mechanism of MBD by TiO_2/mRH-SNP

The first stage of the photocatalytic degradation mechanism of MBD by TiO_2/mRH-SNP involves electron hole pairs

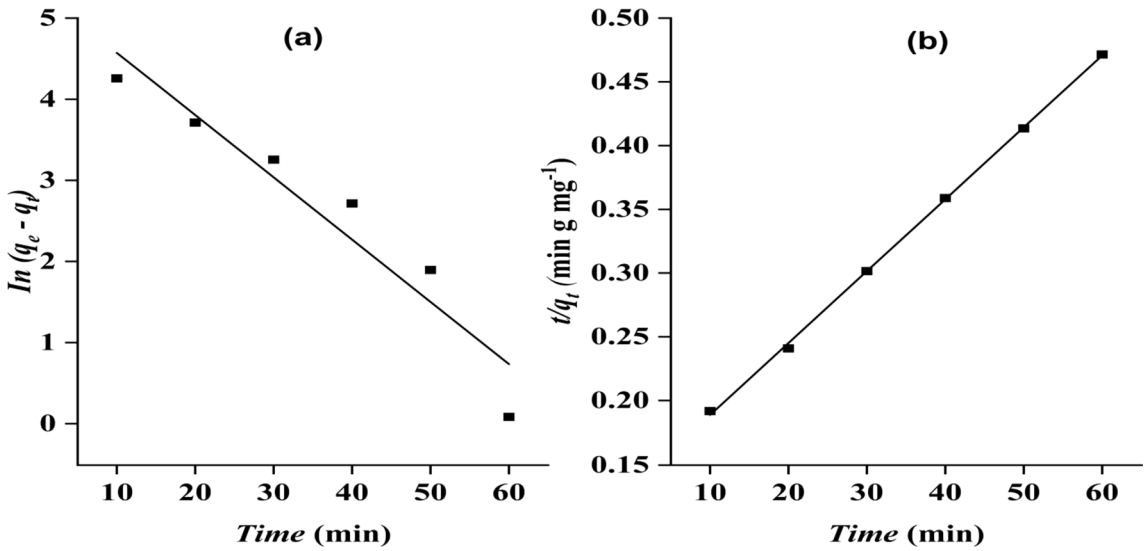

Fig. 9 Kinetic plot of **a** pseudo-first order and **b** pseudo-second order for MBD photodegradation using TiO_2/mRH-SNP

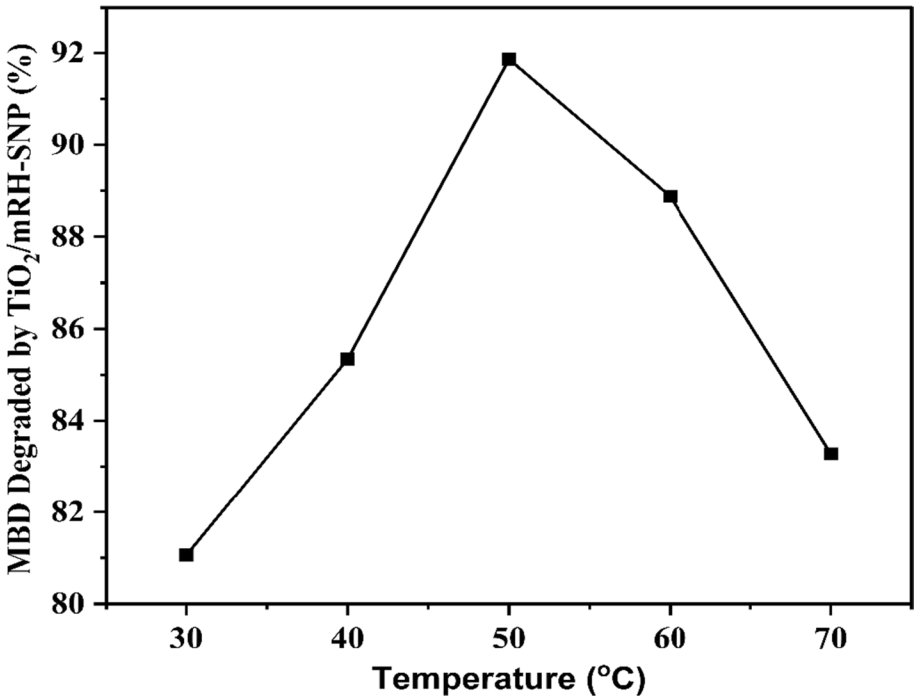

Fig. 10 Temperature effect on MBD photodegradation using TiO_2/mRH-SNP

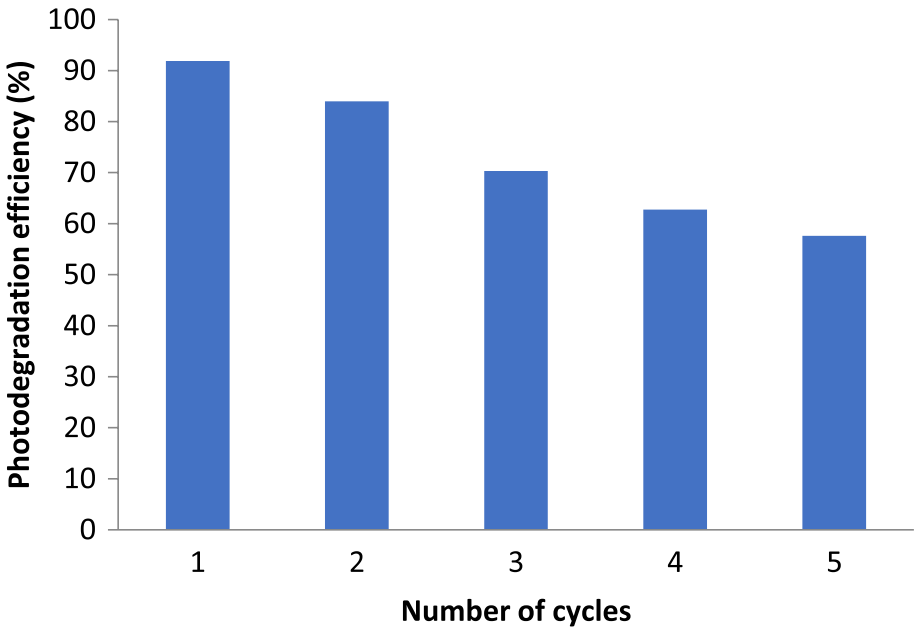

Fig. 11 Influence of TiO_2/mRH-SNP reusability on MBD photodegradation at optimum predicted point

separation influenced by the absorbance of LED light as shown in Eq. (8). The irradiation of the photocatalyst by the LED light separates the electron/pairs. The next mechanism path generates radicals in solution via the oxidation of mRH-SNP ≈ TiO_2 surface bound into hydroxyl radical (·OH) by the valence band hole (h^+) in both materials as presented in Eq. (9). Nonetheless, the electrons present in TiO_2 conduction band recombine with the holes available in the valence band of mRH-SNP and react with oxygen to form reactive superoxide radicals as shown in Eq. (10). Further reaction of superoxide radicals with hydrogen ions in solution and conduction band electron occurs Eq. (11) to form hydrogen peroxide. These radicals (·OH and $\cdot O_2^-$) and H_2O_2 possess excellent reactive and oxidative attributes to effectively degrade MBD molecules into harmless products in the presence of valence band hole as shown in Eq. (12) (Salama et al. 2018).

Table 8 Comparison of previous photocatalysts reusability and stability with present study

Photocatalyst	Pollutant	Reusability number/cycles	Light source	Efficiency reduction	References
TiO_2/mRH-SNP	Methylene blue	5	LED lamp	91.89% to 57.60%	Current study
Reduced graphene oxide-ZnO	Chloramphenicol	4	UV light	87% to 68%	Sodeinde et al. (2022)
CuO@TiO_2	AR8 dye	5	UV light	≈ 90% (<4.5%)	Hamad et al. (2022)
ZnO/pumice composite	Textile dye effluent	5	Sunlight	87.14% to 38.12%	Yusuff et al. (2020)
g-C_3N_4/TiO_2@polyaniline	Congo red	4	Solar light	≈ 100% to 90.1%	Alenizi et al. (2019)
TiO_2@NH_2-MIL-88B(Fe)	Methylene blue	5	LED lamp	99% (Stable)	Li et al. (2018)
g-AP-pAA/TiO2-Au	Methyl violet	5	Sunlight	99% to 90%	Sarkar et al. (2015)

$$\mathrm{mRH-SNP} \approx \mathrm{TiO_2} + \mathrm{hv(LED\ light)} \rightarrow \mathrm{mRH-SNP} \approx \mathrm{TiO_2}\left(h^+\right) + \mathrm{mRH-SNP} \approx \mathrm{TiO_2}\left(e^-\right) \quad (8)$$

$$\mathrm{mRH-SNP} \approx \mathrm{TiO_2} + \mathrm{H_2O} \rightarrow \mathrm{mRH-SNP} \approx \mathrm{TiO_2} + \mathrm{H^+} + \cdot\mathrm{OH} \quad (9)$$

$$\mathrm{O_2} + \mathrm{e^-} \rightarrow \cdot\mathrm{O_2^-} \quad (10)$$

$$2\mathrm{H^+} + \mathrm{e^-} + \cdot\mathrm{O_2^-} \rightarrow \mathrm{H_2O_2} \quad (11)$$

$$\mathrm{MBD} + \cdot\mathrm{OH}, \cdot\mathrm{O_2^-}, \mathrm{H_2O_2}, \mathrm{h^+} \rightarrow \text{degradation products}\ \left(\mathrm{CO_2}, \mathrm{H_2O}, \mathrm{NH_4^+}, \mathrm{SO_4^{2-}}\right) \quad (12)$$

Conclusions

Magnetized TiO_2-supported SiO_2 nanoparticles, synthesized from rice husk, was applied as a photocatalyst to degrade MBD in aqueous solution using LED lamp as light source. Box–Behnken design was employed to design the experiment at varying values of MBD initial concentration, TiO_2 loading, pH and Illumination time. At MBD initial concentration, TiO_2 loading, pH and illumination time of 10 ppm, 15%, 6 and 75 min, respectively, 96.51% of MBD was removed. A correlation coefficient of 0.9569 between predicted and experimental values of PMD substantiates the effectiveness of developed model. ANOVA also revealed high significance and contributory effects of the mathematical model and the examined process parameters on the photodegradation process. Experimental data fitted well into pseudo-second-order kinetic model. The temperature effect revealed optimum MBD photocatalytic degradation at 50 °C by TiO_2/mRH-SNP. Characterization revealed the effects of magnetization and photocatalyst on the synthesized SiO_2 nanoparticles from rice husk. In conclusion, magnetized TiO_2-silica nanoparticles from rice husk could be effectively used to degrade MBD in solution.

Acknowledgements The first author appreciates the support rendered financially by Afe Babalola University, Ado-Ekiti, Nigeria, toward the publication of this article.

Funding No financial support in form of funding was received for the execution of this research work.

Data availability The data used to support the findings of this study are included within the article.

Declarations

Conflict of interest The authors declare no conflict of interest in terms of financial or personal nature for the publication of this article.

Ethical approval This declaration is not applicable.

References

Abbas M, Rao BP, Reddy V, Kima CG (2014) Fe_3O_4/TiO_2 core/shell nanocubes: single-batch surfactant less synthesis, characterization and efficient catalysts form ethylene blue degradation. Ceram Int 40:11177–11186

Abou-Gamra ZM, Ahmed MA, Hamza MA (2017) Investigation of commercial $PbCrO_4$/TiO_2 for photodegradation of rhodamine B in aqueous solution by visible light. Nanotechnol Environ Eng 2:12

Alenizi MA, Kumar R, Aslam M, Alseroury FA, Barakat MA (2019) Construction of a ternary g-C3N4/TiO_2@polyaniline nanocomposite for the enhanced photocatalytic activity under solar light. Sci Rep 9:12091

Bielan Z, Kowalska E, Dudziak S, Wang K, Ohtani B, Zielinska-Jurek A (2020) Mono- and bimetallic (Pt/Cu) titanium(IV) oxide photocatalysts. Physicochemical and photocatalytic data of magnetic nanocomposites' shell. Data Brief 31:105814

Chandrabose G, Dey A, Gaur SS, Pitchaimuthu S, Jagadeesan H, Braithwaite NSJ, Selvaraj V, Kumar V, Krishnamurthy S (2021) Removal and degradation of mixed dye pollutants by integrated adsorption-photocatalysis technique using 2-D MoS_2/TiO_2 nanocomposite. Chemosphere 279:130467

Dagher S, Soliman A, Ziout A, Tit N, Hilal-Alnaqbi A, Khashan S, Alnaimat F, Qudeiri JA (2018) Photocatalytic removal of methylene blue using titania- and silica-coated magnetic nanoparticles. Mater Res Express 5:065518

Długosz O, Staroń A, Brzoza P, Banach M (2022) Synergistic effect of sorption and photocatalysis on the degree of dye removal in single and multicomponent systems on ZnO-SnO_2. Environ Sci Pollut Res 29:27042–27050

Du GH, Liu ZL, Xia X, Chu Q, Zhang SM (2006) Characterization and application of Fe_3O_4/SiO_2 nanocomposites. J Sol-Gel Sci Technol 39:285

Elmorsi TM, Riyad YM, Mohamed ZH, Abid HMH, Bary E (2010) Decolorization of mordant red 73 azo dye in water using H_2O_2/UV photo Fenton treatment. J Hazard Mater 174:352–356

Elsayed SA, El-Sayed IET, Tony MA (2022) Impregnated chitin biopolymer with magnetic nanoparticles to immobilize dye from aqueous media as a simple, rapid and efficient composite photocatalyst. Appl Water Sci 12:252

Fita G, Djakba R, Mouhamadou S, Duc M, Rao S, Popoola LT, Harouna M, Benoit LB (2023) Adsorptive efficiency of hull-based activated carbon toward copper ions (Cu^{2+}) removal from aqueous solution: kinetics, modelling and statistical analysis. Diam Relat Mater 139:110421

Guan S, Yang H, Sun X, Xian T (2020) Preparation and promising application of novel $LaFeO_3$/BiOBr heterojunction photocatalysts for photocatalytic and photo-Fenton removal of dyes. Opt Mater 100:109644

Gul S, Yildlrln OZ (2009) Degradation of Reactive Red 194 and reactive yellow 145 azo dyes by O_3 and H_2O_2/UV-C process. Chem Eng J 155:684–690

Hamad H, Elsenety MM, Sadik W, El-Demerdash A, Nashed A, Mostafa A, Elyamny S (2022) The superior photocatalytic performance and DFT insights of S-scheme CuO@TiO_2 heterojunction composites for simultaneous degradation of organics. Sci Rep 12:2217

Hassan AKM, Dey SC, Rahman MM, Zakaria AM, Sarker M, Ashaduzzaman MD, Shamsuddin MD (2020) A kaolinite/TiO2/ZnO – based novel ternary composite for photocatalytic degradation of anionic azo dyes. Bull Mater Sci 43:27

Herrmann JM (1999) Heterogeneous photocatalysis: fundamentals and applications to the removal of various types of aqueous pollutants. Catal Tod 53(1):115–129

Jamil TS, Ghaly MY, Fathy NA, Abd el-halimOsterlund TAL (2012) Enhancement of TiO_2 behavior on photocatalytic oxidation of MO dye using TiO_2/AC under visible irradiation and sunlight radiation. Sep Purif Technol 98:270–279

Jiménez-Miramontes JA, Domínguez-Arvizu JL, Gaxiola-Cebreros FA, Hernández-Majalca BC, Pantoja-Espinoza JC, Salinas-Gutiérrez JM, Collins-Martínez VH, López-Ortiz A (2022) Effect of the synthesis method on the $MnCO_2O_4$ towards the photocatalytic production of H_2. Rev Adv Mater Sci 61:654–672

Khan MS, García MF, Javed M, Kubacka A, Caudillo-Flores U, Halim SA, Khan A, Al-Harrasi A, Riaz N (2021) Synthesis, characterization, and photocatalytic, bactericidal and molecular docking analysis of Cu−Fe/TiO_2 photocatalysts: influence of metallic impurities and calcination temperature on charge recombination. ACS Omega 6:26108–26118

Lai L, Xie Q, Chi L, Gu W, Wu D (2016) Adsorption of phosphate from water by easily separable Fe_3O_4@SiO_2 core/shell magnetic nanoparticles functionalized with hydrous lanthanum oxide. J Colloid Interface Sci 465:76–82

Latif A, Noor S, Sharif QM, Najeebullah N (2010) Different techniques recently used for the treatment of textile dyeing effluents: a review. J Chem Soc Pak 32(1):115–124

Li Y, Jiang J, Fang Y, Cao Z, Chen D, Li N, Xu Q, Lu J (2018) TiO_2 nanoparticles anchored onto the metal–organic framework NH_2-MIL-88B (Fe) as an adsorptive photocatalyst with enhanced Fenton-like degradation of organic pollutants under visible light irradiation. ACS Sustain Chem Eng 6:16186–16197

Li K, Zhong Y, Luo S, Deng W (2020) Fabrication of powder and modular $H_3PW_{12}O_{40}/Ag_3PO_4$ composites: novel visible-light photocatalysts for ultrafast degradation of organic pollutants in water. Appl Catal B Environ 278:119313

Lim TT, Yap PS, Srinivasan M, Fane AG (2011) TiO_2/AC composites for synergistic adsorption-photocatalysis processes: present challenges and further developments for water treatment and reclamation. Crit Rev Environ Sci Technol 41:1173–1230

Lorenc-Grabowska E, Gryglewicz G (2007) Adsorption characteristics of congo red on coal-based mesoporous activated carbon. Dyes Pigm 74:34–40

Mahross MH, Naggar AH, Elnasr TAS, Abdel-Hakim M (2016) Effect of rice straw extract as an environmental waste corrosion inhibitor on mild steel in an acidic media. Chem Adv Mater 1(1):6–16

Nainani R, Thakur P, Chaskar M (2012) Synthesis of silver doped TiO_2 nanoparticles for the improved photocatalytic degradation of methyl orange. J Mater Sci Eng B 2(1):52–58

Nair AK, George DR, Baby NJ (2021) Solar dye degradation using TiO_2 nanosheet based nanocomposite floating photocatalyst. Mater Today Proc. https://doi.org/10.1016/j.matpr.2021.02.481

Nair AK, JagadeeshBabu BE (2017) Ag-TiO_2 nanosheet embedded photocatalytic membrane for solar water treatment. J Environ Chem Eng 5:4128–4133

Nnodim UJ, Adogwa AA, Akpan UG, Ani IJ (2022) Photocatalytic degradation of methylene blue dye with green zinc oxide doped with nitrogen. J Clin Rheum Res 2(1):59–69

Oyewo OA, Adeniyi A, Sithole BB, Onyango MS (2020) Sawdust based cellulose nanocrystals incorporated with ZnO nanoparticles as efficient adsorption media in the removal of methylene blue dye. ACS Omega 5:18798–18807

Pandit VK, Arbuj SS, Pandit YB, Naik SD, Rane SB, Mulik UP, Gosavic SW, Kale BB (2015) Solar light driven dye degradation using novel organo–inorganic (6,13-Pentacenequinone/TiO_2) nanocomposite. RSC Adv 5:10326–10331

Popoola LT (2019a) Nano-magnetic walnut shell-rice husk for Cd(II) sorption: design and optimization using artificial intelligence and design expert. Heliyon 5:e02381

Popoola LT (2019b) Characterization and adsorptive behaviour of snail shell-rice husk (SS-RH) calcined particles (CPs) towards cationic dye. Heliyon 5:e01153

Popoola LT (2020) Tetracycline and sulfamethoxazole adsorption onto nanomagnetic walnut shell-rice husk: isotherm, kinetic, mechanistic and thermodynamic studies. Int J Environ Anal Chem 100(9):1021–1043

Popoola LT (2023) Efficient Cr(VI) sequestration from aqueous solution by chemically modified Garcinia kola hull particles: characterization, isotherm, kinetic and thermodynamic studies. Environ Sci Pollut Res. https://doi.org/10.1007/s11356-023-29848-0

Popoola LT, Aderibigbe TA, Yusuff AS, Munir MM (2018) Brilliant green dye adsorption onto composite snail shell –rice husk: adsorption isotherm, kinetic, mechanistic and thermodynamic analysis. Environ Qual Manag. https://doi.org/10.1002/tqem.21597

Rashed MN, Eltaher MA, Abdou ANA (2017) Adsorption and photocatalysis for methyl orange and Cd removal from wastewater using TiO2/sewage sludge-based activated carbon nanocomposites. R Soc Open Sci 4:170834

Ravi K, Sathish MB, Satya SG, Manga RI, Basavaiah K, Ventateswan RB (2018) ZnO/RGO nanocomposite via hydrothermal route for photocatalytic degradation of dyes in presence of visible light. Int J Chem Studies 6(6):20–26

Salama A, Mohamed A, Aboamera NM, Osman TA, Khattab A (2018) Photocatalytic degradation of organic dyes using composite nanofibers under UV irradiation. Appl Nanosci 8:155–161

Sarkar AK, Saha A, Panda AB, Pal S (2015) pH Triggered superior selective adsorption and separation of both cationic and anionic dyes and photocatalytic activity on a fully exfoliated titanate layer-natural polymer based nanocomposite. Chem Commun 51(89). https://doi.org/10.1039/c5cc06214d

Sodeinde KO, Olusanya SO, Lawal OS, Sriariyanun M, Adediran AA (2022) Enhanced adsorptional-photocatalytic degradation of chloramphenicol by reduced graphene oxide-zinc oxide nanocomposite. Sci Rep 12:17054

Sridewi N, Lee YF, Sudesh K (2011) Simultaneous adsorption and photocatalytic degradation of malachite green using electrospun P(3HB)-TiO2 nanocomposite fibers and films. Int J Photoenergy 597854:11

Sumanjit TPS, Ravneet WK (2007) Removal of health hazards causing acidic dyes from aqueous solutions by the process of adsorption. Online J Health Allied Sci 6(3):3

Tahoun BA, Mansour S, Tony MA (2022) Development and characterization of conjugated polyaniline/co-doped ZnO nanocomposites for enhanced dye oxidation from wastewater. ERJ Eng Res J 45:101–110

Teixeira S, Delerue-Matos C, Santos L (2012) Removal of sulfamethoxazole from solution by raw and chemically treated walnut shells. Environ Sci Pollut Res 19:3096–3106

Thabet RH, Fouad MK, Sherbiny SAE, Tony MA (2022) Zero-waste approach: assessment of aluminum-based waste as a photocatalyst for industrial wastewater treatment ecology. Int J Environ Res 16:1–19

Thushari I, Babel S (2020) Sustainable utilization of waste palm oil and sulfonated carbon catalyst derived from coconut meal residue for biodiesel production. Bioresour Technol 248:199–203

Tony MA (2022) Valorization of undervalued aluminum-based waterworks sludge waste for the science of "The 5 Rs' criteria". Appl Water Sci 12:1–30

Tony MA, Mansour SA (2020) Solar photo-Fenton reagent with nanostructured iron oxide for Bismarck dye oxidation: an Egyptian apparel case study. Int J Environ Sci Technol 17:1337–1350

Wang XJ, Liu YF, Hu ZH, Chen YJ, Liu W, Zhao GH (2009) Degradation of methyl orange by composite photocatalysts nano-TiO_2 immobilized on activated carbons of different porosities. J Hazard Mater 169:1061–1067

Wang Q, Gao D, Gao C, Wei Q, Cai Y, Xu J, Liu X, Xu Y (2012) Removal of a cationic dye by adsorption/photodegradation using electrospun PAN/O-MMT composite nanofibrous membranes coated with TiO_2. Int J Photoenergy 680419:8

Wei X, Zhu G, Fang J, Chen J (2013) Synthesis, characterization and photocatalysis of well-dispersible phase-pure anatase TiO_2 nanoparticles. Int J Photoenergy 726872:6

Xiao X, Wang Y, Cui B, Zhang X, Zhang D, Xu X (2020) Preparation of MoS_2 nanoflowers with rich active sites as an efficient adsorbent for aqueous organic dyes. New J Chem 44:4558–4567

Xing B, Shi C, Zhang C, Yi G, Chen L, Guo H, Huang G, Cao J. (2016) Preparation of TiO_2/activated carbon composites for photocatalytic degradation of RhB under UV light irradiation. J Nanomaterials 1–10

Yuan H, Xu J (2010) Preparation, characterization and photocatalytic activity of nanometer SnO_2. Int J Chem Eng Appl 1(3):241–246

Yusuff AS, Popoola LT, Aderibigbe EI (2020) Solar photocatalytic degradation of organic pollutants in textile industry wastewater by ZnO/pumice composite photocatalyst. J Environ Chem Eng 8:103907

Yusuff AS, Popoola LT, Anochie V (2021) Utilization of agricultural waste adsorbent for the removal of lead ions from aqueous solutions. Acta Polytechnica 61(4):1–9

Yusuff AS, Popoola LT, Adeniyi DO, Olutoye MA (2022) Coal fly ash supported ZnO catalysed transesterification of Jatropha curcas oil: optimization by response surface methodology. Energy Convers Manag X 16:100302

Zhang S, Zhang Y, Liu J, Xu Q, Xiao H, Wang X, Zhou J (2013) Thiol modified Fe_3O_4@SiO_2 as robust, high effective, and recycling magnetic sorbent for mercury removal. Chem Eng J 226:30–38